Deforestation Strengthens Atmospheric Transport of Mineral Dust and Phosphorus from North Africa to the Amazon

YUE LI,[a] JAMES T. RANDERSON,[a] NATALIE M. MAHOWALD,[b] AND PETER J. LAWRENCE[c]

[a] *Department of Earth System Science, University of California, Irvine, Irvine, California*
[b] *Department of Earth and Atmospheric Sciences, Cornell University, Ithaca, New York*
[c] *Climate and Global Dynamic Laboratory, National Center for Atmospheric Research, Boulder, Colorado*

(Manuscript received 8 October 2020, in final form 19 April 2021)

ABSTRACT: Phosphorus contained in atmospheric mineral dust aerosol originating from Africa fertilizes tropical forests in Amazonia. However, the mechanisms influencing this nutrient transport pathway remain poorly understood. Here we use the Community Earth System Model to investigate how large-scale deforestation affects mineral dust aerosol transport and deposition in the tropics. We find that the surface biophysical changes that accompany deforestation produce a warmer, drier, and windier surface environment that perturbs atmospheric circulation and enhances long-range dust transport from North Africa to the Amazon. Tropics-wide deforestation weakens the Hadley circulation, which then leads to a northward expansion of the Hadley cell and increases surface air pressure over the Sahara Desert. The high pressure anomaly over the Sahara, in turn, increases northeasterly winds across North Africa and the tropical North Atlantic Ocean, which subsequently increases dust transport to the South American continent. We estimate that the annual atmospheric phosphorus deposition from dust significantly increases by 27% ($P < 0.01$) in the Amazon under a scenario of complete deforestation. These interactions exemplify how land surface changes can modify tropical nutrient cycling, which, in turn, may have consequences for long-term changes in tropical ecosystem productivity and biodiversity.

KEYWORDS: Amazon region; Tropics; Hadley circulation; Aerosols; Deforestation; Dust or dust storms

1. Introduction

Deforestation is one of the earliest and most direct disruptions of the natural environment by people (Bonan 2016). It alters local surface air temperature through modifying surface physical properties (Lee et al. 2011; Winckler et al. 2019), increasing greenhouse gas emissions (Houghton 2005), and reducing the sink potential of terrestrial ecosystems (Mahowald et al. 2017; Gasser and Ciais 2013). Over the past several decades, the development of land surface models (Deardorff 1978; Dickinson and Henderson-Sellers 1988) and the representation of the carbon cycle (Potter et al. 1993) in Earth system models has enabled deforestation-driven biophysical and biogeochemical impacts to be quantified and compared with one another at regional to global scales (Pongratz et al. 2010; Bala et al. 2007). Despite these advances, it is rare to see studies exploring the influence of deforestation on atmospheric transport and surface winds, which may indirectly feedback on climate through impacts on nutrient deposition and thus affect net primary production in both remote terrestrial (Swap et al. 1992) and marine ecosystems (Okin et al. 2011).

For the Amazon, North African dust has been identified as one of the key sources for atmospheric deposition of phosphorus (Barkley et al. 2019). Each year, dust from North Africa is transported southwestward along the pathway of tropical easterly trade winds (Washington and Todd 2005). Long-term station records (Prospero et al. 1981) and recent satellite observations (Yu et al. 2015) both indicate that this mineral dust disperses across the Atlantic Ocean and travels as far as South America, where both dry and wet deposition contribute to its deposition in tropical forests (Ridley et al. 2012; Prospero et al. 2020). Other important phosphorus sources in tropical South America include deposition from biomass burning (Mahowald et al. 2005) and Africa (Barkley et al. 2019). Given that tropical soils are highly weathered, it is well established that phosphorus is often a limiting nutrient for net primary production within this biome (Vitousek 1984; Chadwick et al. 1999; Du et al. 2020). Since individual tropical species vary in their phosphorus use strategies in nutrient-poor soils (Hättenschwiler et al. 2008), long-term changes such as increases in phosphorus availability from elevated deposition may contribute to the ecosystem nutrient imbalances, which in turn may affect plant competition and ultimately contribute to negative outcomes for species richness (Wassen et al. 2005) and ecosystem function.

Large-scale changes in dust transport have been linked to climate variability and other forms of global environmental change. Both El Niño (Prospero and Nees 1986) and the positive phase of the North Atlantic Oscillation (NAO) (Moulin et al. 1997) are known to enhance North African dust transport by increasing the magnitude of easterly trade winds across West Africa and the North Atlantic Ocean (Doherty et al. 2012; Evan et al. 2016). On longer time scales, by 2100, climate change is expected to increase North African dust transport as a consequence of increases in surface wind speed in dust source areas (Washington et al. 2009). Dust production from source areas could further change as a consequence of future changes in Sahel rainfall (Biasutti 2013) or CO_2 fertilization of plant growth (Mahowald 2007). In contrast with the impacts of

Supplemental information related to this paper is available at the Journals Online website: https://doi.org/10.1175/JCLI-D-20-0786.s1.

Corresponding author: Yue Li, yue.li@uci.edu

DOI: 10.1175/JCLI-D-20-0786.1

climate change, less work has explored how deforestation modifies dust transport and deposition.

To provide context for interpreting our model experiments, we developed a hypothesis regarding the impact of deforestation on the Hadley circulation, atmospheric dust transport, and nutrient deposition in tropical forests. Our initial theory was that dense equatorial forests across the tropics strengthen the upward branch of regional Hadley circulation (Gedney and Valdes 2000; Snyder 2010) as a consequence of low surface albedo and high levels of surface roughness and evapotranspiration, which, in turn, increase convection and upward vertical velocity over interior tropical continents. In response to the strong outflow in the upper troposphere, the return branch of the Hadley at the surface would be similarly strengthened by strong trade winds, carrying dust and nutrients from extratropical deserts (and savannas) toward equatorial tropical forests. Deposition of phosphorus and other macronutrients and micronutrients, in turn, may sustain tropical forests in regions with highly weathered soils (Chadwick et al. 1999), contributing to a positive feedback loop that simultaneously maintains high levels of tropical forest cover and a robust Hadley circulation. With this proposed mechanism, tropical deforestation would be expected to have the opposite effect on dust transport and would contribute to decreases in phosphorus transport and deposition. As further explored below, this hypothesis mostly draws upon a meridional view of the Hadley circulation and does not consider zonal variations in dust production or atmospheric circulation.

To test multiple aspects of this hypothesis, we conducted idealized experiments using an Earth system model to isolate the impacts of tropical deforestation on atmospheric circulation and dust transport. In our analysis, we focus on the mechanism by which deforestation in the model influences the atmospheric transport and deposition of dust and phosphorus in tropical terrestrial ecosystems. The paper is organized as follows. The model description, experiment design and analysis of model output are described in section 2. In section 3, we report the changes in surface climate, Hadley circulation and dust transport in the tropics from the deforestation experiment. Particular attention is given to the causal chain between simulated tropical deforestation, changes in atmospheric circulation, and subsequent effects on the dust and phosphorus deposition in the Amazon. Section 4 discusses the implications of our findings from these idealized experiments.

2. Methods

a. Model description and experiment design

In our analysis, we used a recently updated version (v2.1.1) of the Community Earth System Model (CESM2) (Danabasoglu et al. 2020) with The Community Atmosphere Model, version 6 (CAM6), coupled with the community land model, version 5 (CLM5). CAM6 uses the same finite-volume (FV) dynamical core as in earlier version and the aerosol module uses the Modal Aerosol Model, version 4 (MAM4; Liu et al. 2016). CLM5 has updated many hydrological and ecological processes (Lawrence et al. 2019) with the accuracy of model output being evaluated by the International Land Model Benchmarking system (Collier et al. 2018). A key slope parameter for the stomatal conductance model in CLM5 is now independent for different plant functional types (PFT), which is expected to better distinguish the transpiration difference between tropical forests and grasslands (Lawrence et al. 2019). The dust model in CLM5 is a mobilization scheme (Mahowald et al. 2006) that accounts for changes in wind friction speed, vegetation cover, and soil moisture based on the Dust Entrainment and Deposition (DEAD) model from Zender et al. (2003).

CESM2 was compiled under a configuration called "F2000climo" with coupled CLM5, CAM6 physics, and a prescribed climatology of sea surface temperatures (SSTs) and sea ice concentrations (SICs) from the observation-based analysis datasets averaged during 1995–2005 (Hurrell et al. 2008). The model has a horizontal spatial resolution of 1.25° × 0.9375° (288 × 192) and 32 vertical levels for the atmospheric model. CLM5 was simulated with prescribed satellite vegetation phenology (CLM5% SP), which enables transpiration and photosynthesis to respond to time-evolving environmental drivers, but with an inactive biogeochemistry. In this configuration, climatological annual cycles of leaf area, stem area, and vegetation heights are prescribed from satellite products (Lawrence et al. 2019) separately for each PFT. The average leaf area index (LAI) and stem area index (SAI) for a grid cell are then computed from a weighted mean of the fraction of each PFT within the grid cell. Atmospheric CO_2 was fixed at the level of 367 ppm.

We performed four coupled experiments with 1) a default PFT map [the control (CTL)], 2) deforestation over the whole tropics (defined as 30°S–30°N) (DEF), 3) deforestation only in tropical America (DEFAme; 30°S–30°N, 117.5°–28.75°W), and 4) deforestation only in tropical Africa (DEFAfr; 30°S–30°N, 27.5°W–55°E). CLM5 divides all terrestrial PFTs into 15 classes and bare soil. To simulate tropical deforestation, we replaced all tropical broadleaf evergreen and deciduous trees (PFT4 and PFT6) with C4 grasses (PFT14) within each grid cell located within the range of latitude and longitude bounds described above. The conversion to C4 grass follows the Land Use Model Intercomparison Project protocol described by Lawrence et al. (2016) and draws upon a long history of treating crop and pasture ecosystems as C4 grass in idealized deforestation simulations (Henderson-Sellers and Gornitz 1984; McGuffie et al. 1995; Swann et al. 2015). Each experiment was run for 100 years with identical boundary conditions for SSTs, SICs, and all other land surface characteristics. We note that this methodology, with 100% (complete) deforestation and 100-yr simulation durations, was made with aim of examining the upper limits of tropical deforestation impacts on dust transport, and with the goal of creating an experimental protocol that allows us to clearly separate deforestation effects from internal climate variability. This design was important for allowing us to investigate mechanisms and test the hypothesis described in the introduction regarding the impact of deforestation on the Hadley circulation, dust, and phosphorus deposition.

b. Analysis of model output

For each experiment, we discarded the first 20 years as spin up and then averaged all variables for the last 80 years. The difference between simulations (i.e., DEF − CTL, DEFAme − CTL, and DEFAfr − CTL) thus represents the climate and

dust response to deforestation across the tropics, and only in tropical America and Africa, respectively. By analyzing the difference between the two simulations, we attempted to reduce (but likely did not eliminate) the influence of biases in the control simulation as it shares the similar simulation biases as the deforestation simulation with respect to the annual cycle of winds, dust concentrations, and aerosol optical depth (AOD). We performed Student's *t* tests to assess 95% confidence levels using each pair of the 80-yr simulated time series. To estimate the uncertainty, one standard deviation was calculated for each 80-yr simulation and then propagated to the subtraction of a pair of simulations (e.g., DEF − CTL).

To quantify the change in the Hadley circulation, we computed changes in zonal-mean airmass streamfunction (Ψ_M):

$$\Psi_M = \frac{2\pi a \cos\phi}{g}\int_p^{\mathrm{PS}} [v]\, dp, \tag{1}$$

where a, ϕ, g, p, and PS denote the radius of Earth, latitude, the acceleration of gravity, pressure, and surface pressure, respectively; $[v]$ is the zonal-mean meridional wind speed. On this basis, Hadley circulation extent was estimated as the position of the 25% of peak values of Ψ_M averaged over the 400–700 hPa pressure range in the Northern Hemisphere, following the definition by Alfaro-Sánchez et al. (2018).

Atmospheric phosphorus deposition from dust was estimated using the following approach:

$$\Delta \mathrm{P}_{\mathrm{deposition|dust}} = \Delta \mathrm{dust}_{\mathrm{deposition}} \times \mathrm{ratio}(\mathrm{P}_{\mathrm{total}}\text{:dust}), \tag{2}$$

where Δ denotes the difference between the DEF and CTL experiments. $\mathrm{dust}_{\mathrm{deposition}}$ is the model simulated total dust deposition, including wet and dry depositions for both the accumulation (26–220 nm, dustbin 1) and coarse (>220 nm, dustbin3) modes. We used a ratio of 770 ppm for the mass ratio of total phosphorus to dust as reported by Wedepohl (1995) from a synthesis of elemental composition data for continental crust to estimate the phosphorus deposition in CESM2. Equation (2) was applied to the difference between the two simulations each month and then aggregated throughout the year to compute the annual deposition in the Amazon basin. We estimated soluble phosphorus from dust as the total phosphorus multiplied by 5% following Barkley et al. (2019).

c. Model evaluation

We used observation-based reanalysis data [the fifth major global reanalysis produced by ECMWF (ERA5; Hersbach et al. 2020); Modern-Era Retrospective Analysis for Research and Applications, version 2 (MERRA-2; Rienecker et al. 2011)] and observations used in previous studies (Albani et al. 2014; Barkley et al. 2019) to evaluate the spatial pattern and seasonal dynamics of atmospheric circulation and dust concentration (and deposition) in CESM2. Previously, CESM has been reported to match dust observations as well as similar aerosol models (e.g., Huneeus et al. 2011). The evaluation in this study shows that CESM2 generally captures some of the large-scale circulation (Fig. S1 in the online supplemental material) and dust transport patterns, as demonstrated by moderate spatial correlations at surface stations with the AOD ($R = 0.54$, $P < 0.001$), surface dust concentration ($R = 0.82$, $P < 0.001$), and dust deposition ($R = 0.87$, $P < 0.001$) (Figs. S2–S4). Comparison with surface dust deposition observations in Fig. S4 and surface concentration measurements from a site near Cayenne, French Guiana (Barkley et al. 2019), in Fig. S5a indicates that CESM2 overestimates dust concentrations in remote environments, particularly during February–April on the northern coast of South America. CESM2 has broad qualitative agreement with AOD and dust annual cycles from MERRA-2 (Figs. S5b–d) for the Amazon. We note that with respect to comparisons with the MERRA-2 reanalysis, AOD from MERRA-2 is observationally constrained by satellite radiance observations, but its dust tracer is not assimilated with same type of constraint. Therefore, while the comparison between CESM2 and MERRA-2 is informative, differences between these two models do not provide a quantitative measure of CESM2 performance. The total dust deposition in the Amazon basin from CESM2 from our control simulation (before deforestation) is $10.0 \pm 2.1\ \mathrm{Tg\ yr^{-1}}$. This estimate is within the range and well below the mean of previous estimates derived from a variety of satellite products and atmospheric models (range: 8–48 $\mathrm{Tg\ yr^{-1}}$; mean: 28 $\mathrm{Tg\ yr^{-1}}$) as shown in Table 2 of Yu et al. (2015).

3. Results

a. Atmospheric drying and surface dust increase

Deforestation causes widespread warming in the tropics (Figs. 1a,b). Large-area replacement of trees with C4 grass decreases vegetation transpiration and surface roughness and increases surface shortwave albedo (Figs. S6a–c). These changes, in turn, contribute to decreases in turbulent energy fluxes (latent and sensible heat fluxes) and increases in outgoing shortwave radiation (Figs. S6d–f). As a consequence of lower evapotranspiration rates and decreases in surface roughness, surface air temperature increases (Fig. 1b and Figs. S6g–i). Mean surface air temperature increases by 0.63° ± 0.07°C across tropical land between 30°S and 30°N, with warming in tropical America (0.87° ± 0.14°C) higher than warming in tropical Africa (0.70° ± 0.11°C) or tropical Asia (0.35° ± 0.08°C). Widespread warming from deforestation is expected and is largely consistent with a large body of literature drawing upon observational analysis (Lee et al. 2011) and simulations that explore deforestation-driven changes in coupling between the land surface and atmosphere (Henderson-Sellers and Gornitz 1984; Lean and Warrilow 1989; Shukla et al. 1990; Costa and Foley 2000; Bala et al. 2007).

In contrast to warming, the rainfall response to deforestation is more spatially heterogeneous (Fig. 1c). Significant declines in precipitation occur in the western Amazon basin and in the Congo, while increases in precipitation occur across the Andes and eastern Amazonia, the Albertine Rift in eastern Africa and the New Guinea Highlands in East Asia. Although there is a consistent tendency of near-surface drying associated with decreases in evapotranspiration across all three continents (indicated by decreases in relative humidity and tropospheric

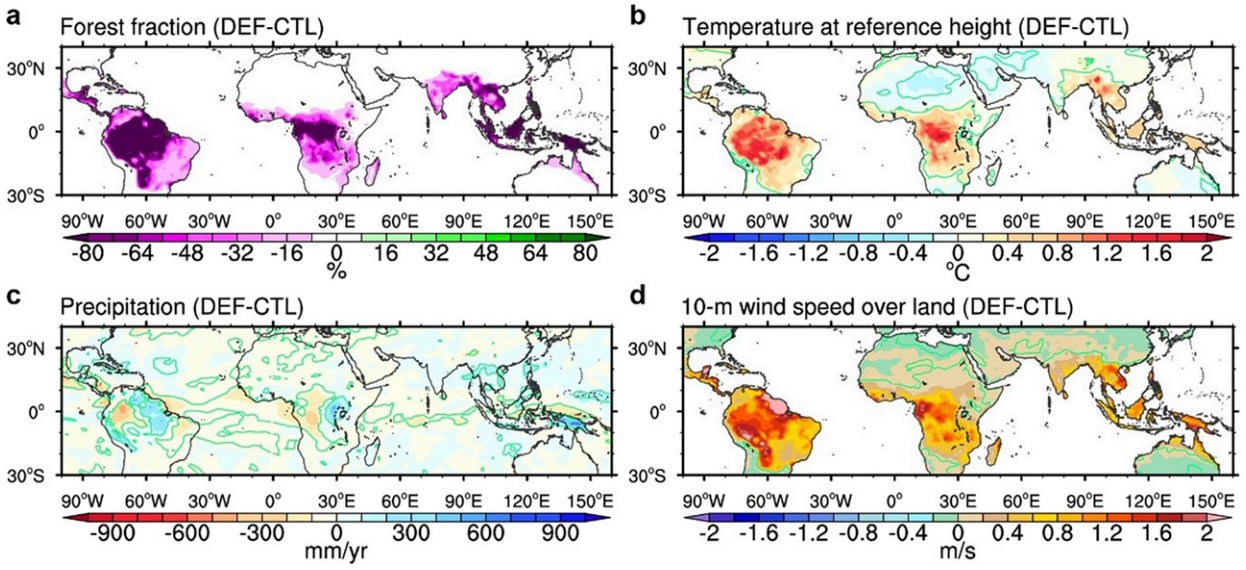

FIG. 1. Tropical deforestation and its influence on surface climate. Annual change in (a) forest fraction (%), (b) surface air temperature at a 2 m reference height (°C), (c) precipitation (mm yr^{-1}), and (d) surface wind speed (m s^{-1}) in response to an idealized simulation of tropical deforestation in the CESM2. The changes were computed as the difference between the mean of 80-yr DEF and CTL simulations. Areas with significant changes ($P < 0.05$) are denoted with green contour lines.

specific humidity between 850 and 700 hPa; Figs. S7 and S8a–d), the precipitation response is complex and likely reflects the impacts of deforestation on interactions between boundary layer processes and regional atmospheric circulation (Spracklen et al. 2018). Key processes that have been identified as contributors to diverging regional precipitation responses from land surface forcing in the tropics include topography (Kooperman et al. 2018), interactions between deep convection and regional jets (Langenbrunner et al. 2019), and atmospheric feedbacks associated with clouds and shortwave radiation (Medvigy et al. 2011; Swann et al. 2015). Over the ocean, we find that deforestation reduces rainfall in the tropical North Atlantic Ocean (Fig. 1c), in a pathway that is particularly important for dust transport from Africa to South America. Surface wind speed over land significantly increases mainly in the area of deforestation (Fig. 1d).

Large-scale deforestation provides a warmer, drier, and windier surface environment for the production and transport of mineral aerosol in the tropics. We find that surface dust emissions significantly increase in the southeastern Sahara and decrease in the north coastal edge of North Africa (Fig. S9b). This is consistent with a southward shift in the location of peak surface dust concentrations, with concentrations and deposition between 0° and 10°N increasing by 9.5% and 7.6%, respectively (Figs. 2a,d and Figs. S9c,d). The deforestation-caused southward shift in surface dust may be partly explained by significant increases in wind speed across the southeastern Sahara (Fig. 1d). Higher dust concentrations also occur in downwind regions, with significant increases in both surface concentration and deposition across the tropical Atlantic Ocean and Amazonia (Figs. 2a,d). Dust deposition across the tropical North Atlantic (0°–10°N) increases by 5.3%, for example, and deposition in the Amazon basin increases by 27% (Figs. S10a,b). Analysis of the mean annual cycle shows that the largest dust increases in Amazonia occur mainly during early spring [February–April, FMA)] (Figs. 2b,e, Figs. S10c,d and S11). The belt of increased dust concentration and deposition stretching from Africa to South America provides evidence that tropical deforestation significantly strengthens the dust transport from the North Africa to the Amazon.

b. *Hadley cell expansion drives enhanced dust transport*

To better understand the physical mechanism of how tropical deforestation influences winds over the North Africa and enhances dust transport over the Atlantic Ocean and South America, we provide more analysis here of deforestation impacts on the Hadley circulation and extratropical circulation. We focus on the early spring (i.e., FMA) period when surface dust concentrations are highest in tropical Africa and South America (Figs. 2b,c). We quantify the change in Hadley circulation using vertical velocity (measuring the upward branch), *u* component of horizontal wind (indicating zonal wind speed for Hadley circulation aloft and near the surface), and zonal-mean airmass streamfunction (see definitions in the methods section). While the general changes of tropical deforestation on mean Hadley cell intensity are small (indicated by the slightly change in air streamfunction in Figs. S8e–h), we find that tropical deforestation produces a northward shift of global and regional Hadley circulation (indicated by increased Hadley cell extent; Table S1). In the tropics, deforestation-induced surface drying reduces the water vapor supply for atmospheric moist convergence, contributing to a negative (downward) vertical velocity anomaly near the equator (Figs. S7b,e and S12). Given the relationship between circulation and vorticity (i.e., circulation per unit area), in combined with the Kelvin's circulation theorem (i.e., constant circulation

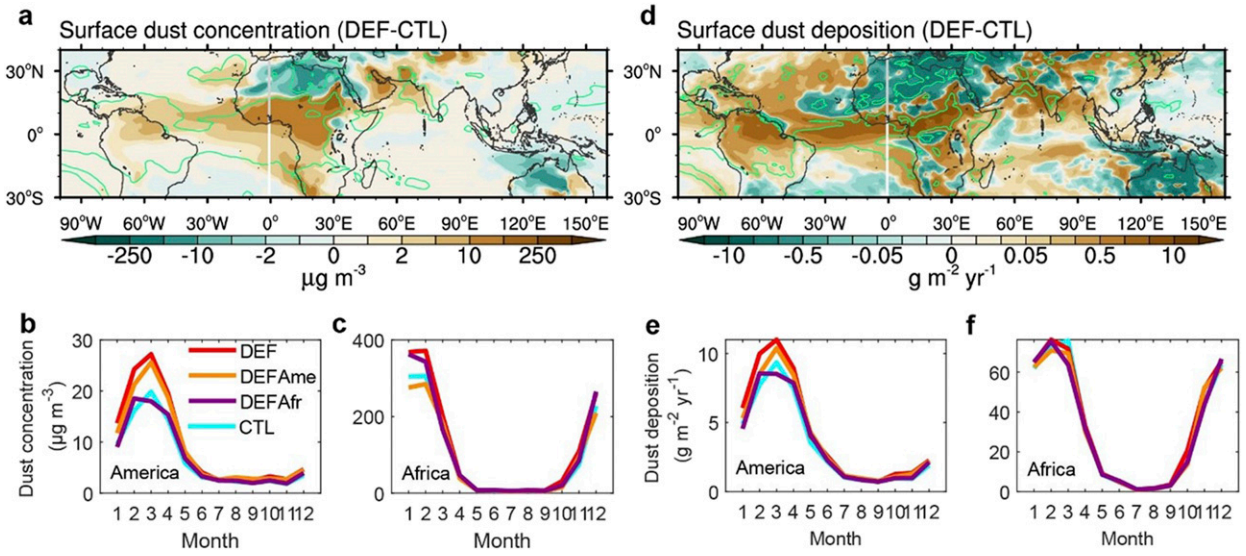

FIG. 2. Annual mean pattern and seasonal distribution of simulated dust concentration and deposition. Annual change (DEF − CTL) in (a) surface dust concentration (μg m^{-3}) and (d) surface dust (wet + dry) deposition (g m^{-2} yr^{-1}). (b),(c) Monthly surface dust concentration from CESM2 simulations over tropical America and Africa, respectively. (e),(f) As in (b) and (c), but for surface dust deposition. The plots in (b)–(f) provide a summary of the mean annual cycle over land regions with forest fraction loss greater than 80% and in tropical areas between 10°S and 10°N. The full ranges of the color bars are −500, −250, −50, −10, −5, −2, −1, 0, 1, 2, 5, 10, 50, 250, and 500 μg m^{-3} for (a) and −30, −10, −5, −1, −0.5, −0.2, −0.1, −0.05, −0.02, −0.01, 0, 0.01, 0.02, 0.05, 0.1, 0.2, 0.5, 1, 5, 10, and 30 g m^{-2} yr^{-1} for (d).

for barotropic ideal fluid with time), the weakened upward branch of Hadley cell and reduced vorticity tend to expand the area of tropical air poleward (see orange color and black arrows in Figs. S12c,d) and this shift of more stable tropical air tends to increase subtropical static stability that has been thought to be close related to the poleward expansion of Hadley circulation (Lu et al. 2007). We also find that deforestation produces a northward shift in subtropical jet stream (Fig. S13), providing additional evidence for a poleward shift in the northern edge of the Hadley cell (Hu and Fu 2007).

When Hadley cell exerts a tendency of moving north, the surface air pressure across the Mediterranean Sea and northern North Africa increases (Fig. 3a, also see Fig. 1d in Alfaro-Sánchez et al. 2018), collocated with the local enhancement of northeasterly wind (Fig. 3b). Further correlation analysis also confirms that a more northward position of Hadley cell extent and enhanced North African northeasterly winds are significantly associated with strengthened FMA dust transport from North Africa to the Amazon in CESM2 (Fig. S14). Key links in the causal chain between simulated tropical deforestation, weakened convection, northward movement of the Hadley cell, and subsequence effects on North African high pressure and enhanced Atlantic dust transport are summarized graphically in Fig. 4.

Additional experiments with CESM2 in which we isolated deforestation to individual continents shows that the increase in dust deposition across Amazonia can be attributed primarily to local deforestation in South America (Figs. 2b,e and 3c,d). Given the climatological easterlies during early spring (Figs. S1c,d), the pressure gradient anomaly between South America and the North Atlantic Ocean caused by deforestation enhances low-level onshore easterlies and dust flow into the Amazon basin (Figs. 3d and 4). Similarly, we find that deforestation in Africa is primarily responsible for the slight increase of surface dust concentration that occurs across northern tropical Africa from January to April (Fig. 2c), a time period previously described as the dust season in the Sahel (Washington and Todd 2005).

c. *Increasing atmospheric phosphorus inputs to the Amazon*

As described above, the dust input to the Amazon largely increases in response to tropical deforestation. To estimate the deforestation-induced phosphorus increase in tropical America, we assumed that the phosphorus mass content of mineral dust aerosol was 770 ppm and that 5% of the total phosphorus was soluble (Wedepohl 1995; Barkley et al. 2019). With these assumptions, we estimate that in the CTL simulation there is an annual total phosphorus deposition flux of 0.0077 ± 0.0016 Tg yr^{-1} and soluble phosphorus flux of 0.0004 ± 0.0001 Tg yr^{-1} over Amazon basin as a consequence of an annual dust deposition of 10.0 ± 2.1 Tg yr^{-1} (Table S2). The DEF − CTL induced increase of total phosphorus is estimated to be 0.0021 ± 0.0024 Tg yr^{-1} ($P < 0.01$, 27 ± 31% relative to the CTL), with soluble phosphorus increasing by 0.0001 ± 0.000 12 Tg yr^{-1}.

The spatial pattern of deposition indicates that the largest phosphorus increase associated with deforestation occurs in the eastern Amazon with a range of 1–5 mg m^{-2} yr^{-1} (Fig. 5a). Relative increases in phosphorus deposition vary from 10% to 40% in the eastern Amazon, and up to 80% in the western Amazon near and along eastern slopes of the Andes mountains (Fig. 5b). According to the phosphorus budget previously

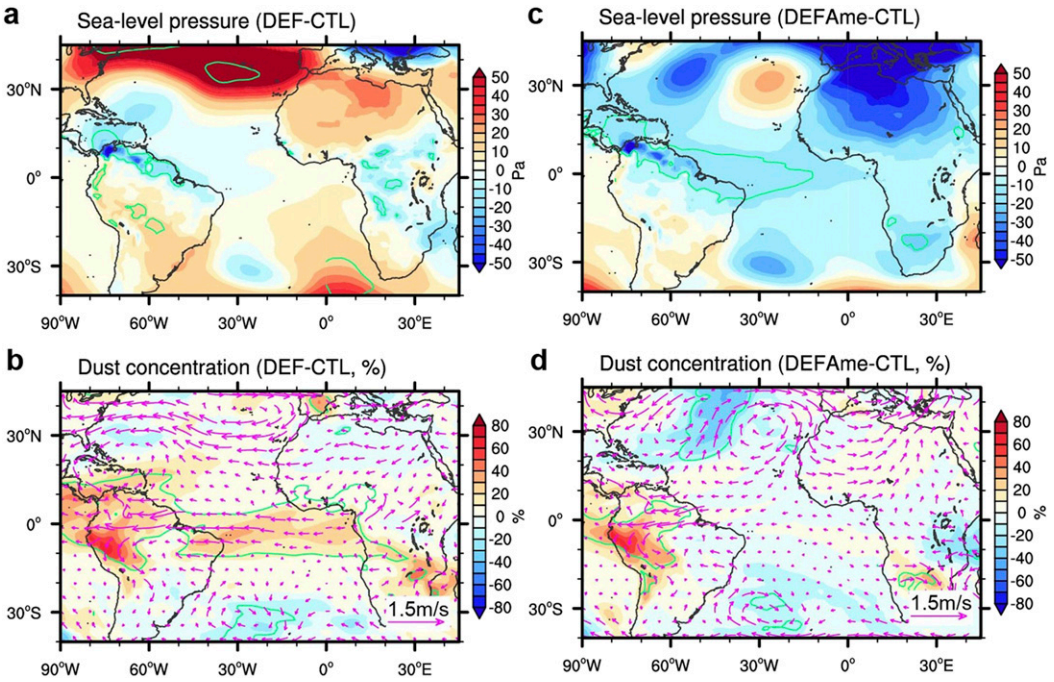

FIG. 3. Low-level tropospheric dust transport from North Africa to the Amazon is strongly controlled by the deforestation-induced atmospheric response during FMA. Change in sea level pressure and low-level tropospheric (defined as 1000–700 hPa average) dust concentration (and horizontal wind) for (a),(b) deforestation in the whole tropics (DEF − CTL); (c),(d) deforestation in tropical America only (DEFAme − CTL). The changes were computed using 80-yr FMA means with areas surrounded by a green line denoting significant changes at a $P < 0.05$ level. Magenta vectors in (b) and (d) denote the changes in low-level tropospheric horizontal winds averaged between 10 000 and 700 hPa ($m\,s^{-1}$). Change in dust concentration is reported as a percentage relative to the CTL value.

reported in Rio Negro basin of Amazonia by Gardner (1990), the sum of phosphorus from atmospheric input of 19.5 $mg\,m^{-2}\,yr^{-1}$ and from soil weathering of 7.5 $mg\,m^{-2}\,yr^{-1}$ almost balance the phosphorus loss from riverine export (27.3 $mg\,m^{-2}\,yr^{-1}$). In the context of this budget, our simulations indicate that the circulation change by deforestation could increase the total phosphorus from dust by 1.0 $mg\,m^{-2}\,yr^{-1}$ (average over 4°S–2°N, 68°–60°W), equivalent to about 13% of the estimated phosphorus flux from weathering.

4. Discussion and implications

Disentangling the complex interaction among land surface biophysical changes, response in atmospheric circulation, nutrient cycling is fundamental to future ecosystem management and our understanding of the long-term effects of deforestation on tropical ecosystem function. In this study, we show that tropical deforestation enhances atmospheric dust transport to the Amazon. Tropical deforestation, collocated with declines in surface turbulent fluxes and increased albedo, has long been known to reduce regional moisture convergence (Lean and Warrilow 1989; Shukla et al. 1990) and weaken tropical circulation (Gedney and Valdes 2000; Snyder 2010). Our CESM2 simulations reproduce these biophysical climate effects and confirm their importance, and our analysis further shows that deforestation weakens the upward branch of Hadley circulation. Following our hypothesis, we expected that the weakened tropical circulation would reduce the strength of trade winds and weaken dust transport from North Africa to the Amazon. However, contrary to our initial hypothesis, the model also simulates a tendency of tropical expansion (i.e., increased Hadley cell extent), likely from by the poleward propagation of tropical static stability. This Hadley cell adjustment, more than the simple weakening in the deep tropics, triggers a series of changes in surface winds and dust transport that increases dust deposition and nutrient deposition. Specifically, our results show that even a slight northward movement of the northern edge of the Hadley circulation can increase the surface pressure and northeasterly winds in North Africa, which is consistent with previous identification of the Libyan high pressure system for the enhancement of North African dust transport (Washington and Todd 2005). This perturbation over the North African dust source region, combined with deforestation-induced near-surface drying and increased wind speeds, causes dust to be more easily transported from North Africa to the Amazon (Fig. S15). Our finding thus provides model evidence that the response in Hadley circulation position caused by deforestation may, in turn, increase coupling between Africa and the South America, and lead to increases in dust deposition in the Amazon.

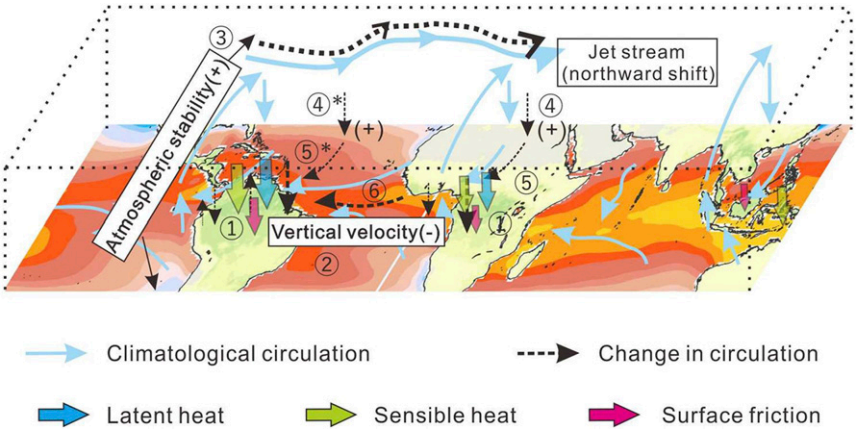

FIG. 4. A diagram showing deforestation-induced changes in atmospheric circulation and dust transport during early North Hemisphere spring (FMA). Deforestation in the tropics causes a cascade of changes in atmospheric circulation: Step 1 involves widespread decreases in surface latent and sensible heat fluxes as a consequence of albedo increases and transpiration and aerodynamic roughness decreases. In step 2 there is a weakening of the upward branch of Hadley cell. Step 3 is a more stable tropical atmosphere that causes the Hadley cell edge and jet stream to shift northward. In steps 4 and 5 large-scale shifts in subtropical circulation increase northern North Africa sea level pressure and enhance North African northeasterly winds. In step 6 further enhancements in northeasterly winds across the tropical North Atlantic strengthen transport from North Africa to the Amazon. In the diagram SSTs are shown over the ocean and leaf area index is shown over the land surface.

The mechanism of dust effect by deforestation identified in this study is also helpful for understanding the climate controls on the interannual variability of observed dust transport from North Africa. Previous studies have provided observational evidence of the Atlantic dust variability being positively linked to a series of climate indices [El Niño (Prospero and Nees 1986); positive phase of NAO (Moulin et al. 1997)] and enhanced northeasterlies in North Africa coincident with the movement of the intertropical convergence zone over West Africa (Doherty et al. 2012; Evan et al. 2016). Here we find that a surface high pressure anomaly across the Mediterranean Sea and northern North Africa enhances North African northeasterly winds and its dust transport across the Atlantic in the deforestation experiment. The surface pressure response to deforestation is consistent with the spatial pattern of the positive NAO index (Hurrell 1995). Our simulations suggest that the coupled Earth system model can be a useful tool for projecting future changes in tropical dust transport and nutrient cycling.

There is additional work needed to examine how changes in tropical tree cover are likely to change dust transport and circulation patterns (and to evaluate our hypothesis). These include 1) testing with other models including those participating in the Land Use Model Intercomparison Project (LUMIP) (Lawrence et al. 2016); 2) considering a fully coupled simulation with an interactive ocean that would allow for additional perturbations to local changes in sea surface temperatures across the North Atlantic Ocean and surface air pressure across the North Africa; 3) assessing interactions between deforestation, increasing greenhouse gases, and aerosols for dust transport and nutrient deposition; and 4) verifying the potential impacts of historical deforestation on transport and nutrient cycling in the tropics. In particular, within the current Land-Use Harmonization v2h (LUHv2h) dataset (Hurtt et al. 2020), approximately 6% of the Amazon basin forests has been cumulatively lost during 1850–2015. Making the simple assumption that our results would scale linearly, this would yield a 1.6% (6% × 27%) increase in phosphorus deposition during the historical period. While small, our results highlight the potential for future anthropogenic land-cover change to strengthen the circulation and dust pathways linking Africa and the Amazon.

In terms of the anthropogenic impacts on the atmospheric phosphorus budget, deforestation fires have been previously identified as an important emissions source (Wang et al. 2015). Our findings highlight another pathway by which deforestation can modify nutrient availability, by strengthening the mineral dust teleconnection between Africa and the Amazon (Barkley et al. 2019). Although our focus here was on phosphorus, deforestation-driven increases in northeasterly trade winds during early spring across the tropical North Atlantic would also likely increase delivery of iron and other micronutrients to the North Atlantic Ocean from both dust and biomass burning in the North Africa. Although the circulation-induced annual increase in atmospheric phosphorus from dust is a small component of net atmospheric phosphorus deposition in Amazonian forests (e.g., Gardner 1990), it represents a new source that is distinct from other larger components that are likely associated with recycling between the biosphere and atmosphere, including, for example, phosphorus cycling associated with spores. As a result, increases in the mineral dust source of phosphorus may contribute to changes in ecosystem

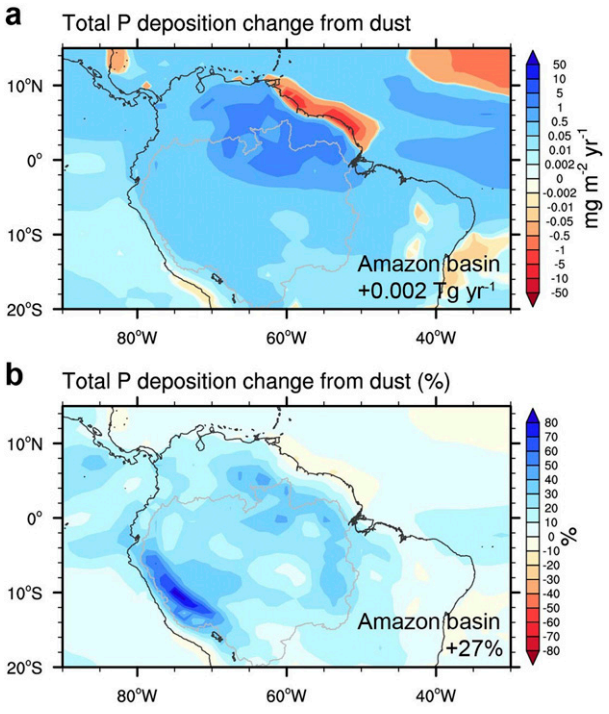

FIG. 5. Annual phosphorus deposition increases in the Amazon as a consequence of tropical deforestation (DEF − CTL). The estimation assumes that the mass ratio of phosphorus in mineral dust aerosol was 770 ppm as indicated by Wedepohl (1995). The gray line shows the boundary of Amazon basin where the annual mineral dust and phosphorus deposition were reported in this study.

function that emerge on longer (millennial) time scales since tropical forest soils are often highly weathered (Chadwick et al. 1999). In the broader context of global environmental change, our results contribute to an improved understanding of how humans are influencing the long-term evolution of biogeochemical–climate interactions.

Acknowledgments. Y. L. and J. T. R. acknowledge support from the U.S. Department of Energy (DOE) Office of Science, Biological and Environmental Research, Earth and Environmental Systems Modeling program to study dust and fire (DE-SC0021302) and the RUBISCO Scientific Focus Area. N. M. M. acknowledges the support from a DOE Office of Science grant (DE-SC0006791) to Cornell. CESM development is led by the National Center for Atmospheric Research (NCAR) and supported by the U.S. National Science Foundation (NSF) and DOE. CESM simulations were run at the DOE National Energy Research Scientific Computing Center (NERSC) on Cori system (project: m2467).

Data availability statement. ERA5 and MERRA-2 data can be downloaded from the Copernicus Climate Change Service (C3S) Climate Date Store (https://cds.climate.copernicus.eu/#!/search?text=ERA5&type=dataset) and the NASA Goddard Earth Science (GES) Data and Information Services Center (DISC) (https://gmao.gsfc.nasa.gov/reanalysis/MERRA-2/data_access/). Model output from the CESM2 tropical deforestation experiments is stored on the data servers of cscratch1 directory on Cori system in DOE National Energy Research Scientific Computing Center (NERSC). The code used for analysis and illustration is available from the corresponding author upon request.

REFERENCES

Albani, S., and Coauthors, 2014: Improved dust representation in the Community Atmosphere Model. *J. Adv. Model. Earth Syst.*, **6**, 541–570, https://doi.org/10.1002/2013MS000279.

Alfaro-Sánchez, R., and Coauthors, 2018: Climatic and volcanic forcing of tropical belt northern boundary over the past 800 years. *Nat. Geosci.*, **11**, 933–938, https://doi.org/10.1038/s41561-018-0242-1.

Bala, G., K. Caldeira, M. Wickett, T. J. Phillips, D. B. Lobell, C. Delire, and A. Mirin, 2007: Combined climate and carbon-cycle effects of large-scale deforestation. *Proc. Natl. Acad. Sci. USA*, **104**, 6550–6555, https://doi.org/10.1073/pnas.0608998104.

Barkley, A. E., and Coauthors, 2019: African biomass burning is a substantial source of phosphorus deposition to the Amazon, tropical Atlantic Ocean, and Southern Ocean. *Proc. Natl. Acad. Sci. USA*, **116**, 16 216–16 221, https://doi.org/10.1073/pnas.1906091116.

Biasutti, M., 2013: Forced Sahel rainfall trends in the CMIP5 archive. *J. Geophys. Res. Atmos.*, **118**, 1613–1623, https://doi.org/10.1002/jgrd.50206.

Bonan, G. B., 2016: Forests, climate, and public policy: A 500-year interdisciplinary odyssey. *Annu. Rev. Ecol. Evol. Syst.*, **47**, 97–121, https://doi.org/10.1146/annurev-ecolsys-121415-032359.

Chadwick, O. A., L. A. Derry, P. M. Vitousek, B. J. Huebert, and L. O. Hedin, 1999: Changing sources of nutrients during four million years of ecosystem development. *Nature*, **397**, 491–497, https://doi.org/10.1038/17276.

Collier, N., F. M. Hoffman, D. M. Lawrence, G. Keppel-Aleks, C. D. Koven, W. J. Riley, M. Mu, and J. T. Randerson, 2018: The International Land Model Benchmarking (ILAMB) system: Design, theory, and implementation. *J. Adv. Model. Earth Syst.*, **10**, 2731–2754, https://doi.org/10.1029/2018MS001354.

Costa, M. H., and J. A. Foley, 2000: Combined effects of deforestation and doubled atmospheric CO_2 concentrations on the climate of Amazonia. *J. Climate*, **13**, 18–34, https://doi.org/10.1175/1520-0442(2000)013<0018:CEODAD>2.0.CO;2.

Danabasoglu, G., and Coauthors, 2020: The Community Earth System Model version 2 (CESM2). *J. Adv. Model. Earth Syst.*, **12**, e2019MS001916, https://doi.org/10.1029/2019MS001916.

Deardorff, J. W., 1978: Efficient prediction of ground surface temperature and moisture, with inclusion of a layer of vegetation. *J. Geophys. Res.*, **83**, 1889–1903, https://doi.org/10.1029/JC083iC04p01889.

Dickinson, R. E., and A. Henderson-Sellers, 1988: Modelling tropical deforestation: A study of GCM land-surface parametrizations. *Quart. J. Roy. Meteor. Soc.*, **114**, 439–462, https://doi.org/10.1002/qj.49711448009.

Doherty, O. M., N. Riemer, and S. Hameed, 2012: Control of Saharan mineral dust transport to Barbados in winter by the intertropical convergence zone over West Africa. *J. Geophys. Res.*, **117**, D19117, https://doi.org/10.1029/2012JD017767.

Du, E., and Coauthors, 2020: Global patterns of terrestrial nitrogen and phosphorus limitation. *Nat. Geosci.*, **13**, 221–226, https://doi.org/10.1038/s41561-019-0530-4.

Evan, A. T., C. Flamant, M. Gaetani, and F. Guichard, 2016: The past, present and future of African dust. *Nature*, **531**, 493–495, https://doi.org/10.1038/nature17149.

Gardner, L. R., 1990: The role of rock weathering in the phosphorus budget of terrestrial watersheds. *Biogeochemistry*, **11**, 97–110, https://doi.org/10.1007/BF00002061.

Gasser, T., and P. Ciais, 2013: A theoretical framework for the net land-to-atmosphere CO_2 flux and its implications in the definition of "emissions from land-use change." *Earth Syst. Dyn.*, **4**, 171–186, https://doi.org/10.5194/esd-4-171-2013.

Gedney, N., and P. J. Valdes, 2000: The effect of Amazonian deforestation on the Northern Hemisphere circulation and climate. *Geophys. Res. Lett.*, **27**, 3053–3056, https://doi.org/10.1029/2000GL011794.

Hättenschwiler, S., B. Aeschlimann, M. M. Coûteaux, J. Roy, and D. Bonal, 2008: High variation in foliage and leaf litter chemistry among 45 tree species of a neotropical rainforest community. *New Phytol.*, **179**, 165–175, https://doi.org/10.1111/j.1469-8137.2008.02438.x.

Henderson-Sellers, A., and V. Gornitz, 1984: Possible climatic impacts of land cover transformations, with particular emphasis on tropical deforestation. *Climatic Change*, **6**, 231–257, https://doi.org/10.1007/BF00142475.

Hersbach, H., and Coauthors, 2020: The ERA5 global reanalysis. *Quart. J. Roy. Meteor. Soc.*, **146**, 1999–2049, https://doi.org/10.1002/qj.3803.

Houghton, R. A., 2005: Tropical deforestation as a source of greenhouse gas emissions. *Tropical Deforestation and Climate Change*, P. Moutinho and S. Schwartzman, Eds., Amazon Institute for Environmental Research, 13–21.

Hu, Y., and Q. Fu, 2007: Observed poleward expansion of the Hadley circulation since 1979. *Atmos. Chem. Phys.*, **7**, 5229–5236, https://doi.org/10.5194/acp-7-5229-2007.

Huneeus, N., and Coauthors, 2011: Global dust model intercomparison in AeroCom phase I. *Atmos. Chem. Phys.*, **11**, 7781–7816, https://doi.org/10.5194/acp-11-7781-2011.

Hurrell, J. W., 1995: Decadal trends in the North Atlantic Oscillation: Regional temperatures and precipitation. *Science*, **269**, 676–679, https://doi.org/10.1126/science.269.5224.676.

——, J. J. Hack, D. Shea, J. M. Caron, and J. Rosinski, 2008: A new sea surface temperature and sea ice boundary dataset for the Community Atmosphere Model. *J. Climate*, **21**, 5145–5153, https://doi.org/10.1175/2008JCLI2292.1.

Hurtt, G. C., and Coauthors, 2020: Harmonization of global land use change and management for the period 850–2100 (LUH2) for CMIP6. *Geosci. Model Dev.*, **13**, 5425–5464, https://doi.org/10.5194/gmd-13-5425-2020.

Kooperman, G. J., Y. Chen, F. M. Hoffman, C. D. Koven, K. Lindsay, M. S. Pritchard, A. L. S. Swann, and J. T. Randerson, 2018: Forest response to rising CO_2 drives zonally asymmetric rainfall change over tropical land. *Nat. Climate Change*, **8**, 434–440, https://doi.org/10.1038/s41558-018-0144-7.

Langenbrunner, B., M. S. Pritchard, G. J. Kooperman, and J. T. Randerson, 2019: Why does Amazon precipitation decrease when tropical forests respond to increasing CO_2? *Earth's Future*, **7**, 450–468, https://doi.org/10.1029/2018EF001026.

Lawrence, D. M., and Coauthors, 2016: The Land Use Model Intercomparison Project (LUMIP) contribution to CMIP6: Rationale and experimental design. *Geosci. Model Dev.*, **9**, 2973–2998, https://doi.org/10.5194/gmd-9-2973-2016.

——, and Coauthors, 2019: The Community Land Model version 5: Description of new features, benchmarking, and impact of forcing uncertainty. *J. Adv. Model. Earth Syst.*, **11**, 4245–4287, https://doi.org/10.1029/2018MS001583.

Lean, J., and D. A. Warrilow, 1989: Simulation of the regional climatic impact of Amazon deforestation. *Nature*, **342**, 411–413, https://doi.org/10.1038/342411a0.

Lee, X., and Coauthors, 2011: Observed increase in local cooling effect of deforestation at higher latitudes. *Nature*, **479**, 384–387, https://doi.org/10.1038/nature10588.

Liu, X., P.-L. Ma, H. Wang, S. Tilmes, B. Singh, R. C. Easter, S. J. Ghan, and P. J. Rasch, 2016: Description and evaluation of a new four-mode version of the Modal Aerosol Module (MAM4) within version 5.3 of the Community Atmosphere Model. *Geosci. Model Dev.*, **9**, 505–522, https://doi.org/10.5194/gmd-9-505-2016.

Lu, J., G. A. Vecchi, and T. Reichler, 2007: Expansion of the Hadley cell under global warming. *Geophys. Res. Lett.*, **34**, L06805, https://doi.org/10.1029/2006GL028443.

Mahowald, N. M., 2007: Anthropocene changes in desert area: Sensitivity to climate model predictions. *Geophys. Res. Lett.*, **34**, L18817, https://doi.org/10.1029/2007GL030472.

——, P. Artaxo, A. R. Baker, T. D. Jickells, G. S. Okin, J. T. Randerson, and A. R. Townsend, 2005: Impacts of biomass burning emissions and land use change on Amazonian atmospheric phosphorus cycling and deposition. *Global Biogeochem. Cycles*, **19**, GB4030, https://doi.org/10.1029/2005GB002541.

——, D. R. Muhs, S. Levis, P. J. Rasch, M. Yoshioka, C. S. Zender, and C. Luo, 2006: Change in atmospheric mineral aerosols in response to climate: Last glacier period, preindustrial, modern, and doubled carbon dioxide climates. *J. Geophys. Res.*, **111**, D10202, https://doi.org/10.1029/2005JD006653.

——, and Coauthors, 2017: Interactions between land use change and carbon cycle feedbacks. *Global Biogeochem. Cycles*, **31**, 96–113, https://doi.org/10.1002/2016GB005374.

McGuffie, K., A. Henderson-Sellers, H. Zhang, T. B. Durbidge, and A. J. Pitman, 1995: Global climate sensitivity to tropical deforestation. *Global Planet. Change*, **10**, 97–128, https://doi.org/10.1016/0921-8181(94)00022-6.

Medvigy, D., R. L. Walko, and R. Avissar, 2011: Effects of deforestation on spatiotemporal distributions of precipitation in South America. *J. Climate*, **24**, 2147–2163, https://doi.org/10.1175/2010JCLI3882.1.

Moulin, C., C. E. Lambert, F. Dulac, and U. Dayan, 1997: Control of atmospheric export of dust from North Africa by the North Atlantic Oscillation. *Nature*, **387**, 691–694, https://doi.org/10.1038/42679.

Okin, G. S., and Coauthors, 2011: Impacts of atmospheric nutrient deposition on marine productivity: Roles of nitrogen, phosphorus, and iron. *Global Biogeochem. Cycles*, **25**, GB2022, https://doi.org/10.1029/2010GB003858.

Pongratz, J., C. H. Reick, T. Raddatz, and M. Claussen, 2010: Biogeophysical versus biogeochemical climate response to historical anthropogenic land cover change. *Geophys. Res. Lett.*, **37**, L08702, https://doi.org/10.1029/2010GL043010.

Potter, C. S., J. T. Randerson, C. B. Field, P. A. Matson, P. M. Vitousek, H. A. Mooney, and S. A. Klooster, 1993: Terrestrial ecosystem production: A process model based on global satellite and surface data. *Global Biogeochem. Cycles*, **7**, 811–841, https://doi.org/10.1029/93GB02725.

Prospero, J. M., and R. T. Nees, 1986: Impact of the North African drought and El Niño on mineral dust in the Barbados trade winds. *Nature*, **320**, 735–738, https://doi.org/10.1038/320735a0.

——, R. A. Glaccum, and R. T. Nees, 1981: Atmospheric transport of soil dust from Africa to South America. *Nature*, **289**, 570–572, https://doi.org/10.1038/289570a0.

——, and A. E. Barkley, C. J. Gaston, A. Gatineau, A. Campos y Sansano, and K. Panechou, 2020: Characterizing and quantifying African dust transport and deposition to South America: Implications for the phosphorus budget in the Amazon basin. *Global Biogeochem. Cycles*, **34**, e2020GB006536, https://doi.org/10.1029/2020GB006536.

Ridley, D. A., C. L. Heald, and B. Ford, 2012: North African dust export and deposition: A satellite and model perspective. *J. Geophys. Res.*, **117**, D02202, https://doi.org/10.1029/2011JD016794.

Rienecker, M. M., and Coauthors, 2011: MERRA: NASA's Modern-Era Retrospective Analysis for Research and Applications. *J. Climate*, **24**, 3624–3648, https://doi.org/10.1175/JCLI-D-11-00015.1.

Shukla, J., C. Nobre, and P. Sellers, 1990: Amazon deforestation and climate change. *Science*, **247**, 1322–1325, https://doi.org/10.1126/science.247.4948.1322.

Snyder, P. K., 2010: The influence of tropical deforestation on the Northern Hemisphere climate by atmospheric teleconnections. *Earth Interact.*, **14**, https://doi.org/10.1175/2010EI280.1.

Spracklen, D. V., J. C. A. Baker, L. Garcia-Carreras, and J. H. Marsham, 2018: The effects of tropical vegetation on rainfall. *Annu. Rev. Environ. Resour.*, **43**, 193–218, https://doi.org/10.1146/annurev-environ-102017-030136.

Swann, A. L., M. Longo, R. G. Knox, E. Lee, and P. R. Moorcroft, 2015: Future deforestation in the Amazon and consequences for South American climate. *Agric. For. Meteor.*, **214**, 12–24, https://doi.org/10.1016/j.agrformet.2015.07.006.

Swap, R., M. Garstang, S. Greco, R. Talbot, and P. Kållberg, 1992: Saharan dust in the Amazon basin. *Tellus*, **44B**, 133–149, https://doi.org/10.3402/tellusb.v44i2.15434.

Vitousek, P. M., 1984: Litterfall, nutrient cycling, and nutrient limitation in tropical forests. *Ecology*, **65**, 285–298, https://doi.org/10.2307/1939481.

Wang, R., Y. Balkanski, O. Boucher, P. Ciais, J. Peñuelas, and S. Tao, 2015: Significant contribution of combustion-related emissions to the atmospheric phosphorus budget. *Nat. Geosci.*, **8**, 48–54, https://doi.org/10.1038/ngeo2324.

Washington, R., and M. C. Todd, 2005: Atmospheric controls on mineral dust emission from the Bodélé Depression, Chad: The role of the low level jet. *Geophys. Res. Lett.*, **32**, L17701, https://doi.org/10.1029/2005GL023597.

——, and Coauthors, 2009: Dust as a tipping element: The Bodélé Depression, Chad. *Proc. Natl. Acad. Sci. USA*, **106**, 20 564–20 571, https://doi.org/10.1073/pnas.0711850106.

Wassen, M. J., H. O. Venterink, E. D. Lapshina, and F. Tanneberger, 2005: Endangered plants persist under phosphorus limitation. *Nature*, **437**, 547–550, https://doi.org/10.1038/nature03950.

Wedepohl, K. H., 1995: The composition of the continental crust. *Geochim. Cosmochim. Acta*, **59**, 1217–1232, https://doi.org/10.1016/0016-7037(95)00038-2.

Winckler, J., and Coauthors, 2019: Different response of surface temperature and air temperature to deforestation in a climate model. *Earth Syst. Dyn.*, **10**, 473–484, https://doi.org/10.5194/esd-10-473-2019.

Yu, H., and Coauthors, 2015: The fertilizing role of African dust in the Amazon rainforest: A first multiyear assessment based on data from Cloud-Aerosol Lidar and Infrared Pathfinder Satellite Observations. *Geophys. Res. Lett.*, **42**, 1984–1991, https://doi.org/10.1002/2015GL063040.

Zender, C. S., H. Bian, and D. Newman, 2003: Mineral Dust Entrainment and Deposition (DEAD) model: Description and 1990s dust climatology. *J. Geophys. Res.*, **108**, 4416, https://doi.org/10.1029/2002JD002775.